Contrib. Astron. Obs. Skalnaté Pleso **48**, 356 – 380, (2018)

Numerical simulation of asteroid system dynamics

V.V. Troianskyi[1] **and O.A. Bazyey**[2]

[1] *Astronomical Observatory of Odessa I.I. Mechnikov National University, Odessa, Ukraine, (E-mail: v.troianskyi@onu.edu.ua)*

[2] *Department of Theoretical Physics and Astronomy of Odessa I.I. Mechnikov National University, Odessa, Ukraine*

Received: March 29, 2018; Accepted: April 24, 2018

Abstract. This paper describes a numerical simulation model of motion of moonlets in binary and multiple asteroid systems. Gravitational accelerations produced by the primary body, its moonlets, the Sun, the Moon, and eight major planets are accounted for in this model. The asymmetry of the primary and the effects of solar radiation pressure on the moons in asteroid systems are also factored in. To run the numerical simulation, we adopted the orbital state vectors of celestial bodies from the numerical theory. Using Keplerian orbital elements of the primaries of asteroid systems, we determined their heliocentric positions. Differential equations of motion of celestial bodies in asteroid systems were solved in the asteroid-centric Cartesian reference frame by the Everhart 15th-order method of integration. The verification and validation of the simulation model have been performed for three asteroid systems, namely (136617) 1994 CC and (87) Sylvia, which belong to the near-Earth and main belt populations, respectively, and (136108) Haumea, which is a trans-Neptunian object. These are three asteroid systems of almost 300 small Solar-system bodies with discovered moons which are known to date. All six Keplerian orbital elements determined with reasonable accuracy are available for all asteroid moons.

Key words: N-body simulations – minor planets – asteroids

1. Introduction

Different methods for numerical integration of equations of motion of celestial bodies have been developed and applied to solve a variety of problems of celestial mechanics. A good few authors are currently presenting various numerical models for integration of equations of small-body motion. One of these authors, Sverre J. Aarseth, in his book "Gravitational N-Body Simulations" (Aarseth, 2003) discusses different procedures of numerical integration in the Solar System, circumstellar environment, the Galaxy and interstellar medium. The book also describes all possible options for the integration step size control, as well as different integration methods.

With regard to multiple asteroid systems, their numerical models tend to consist of two, three or more bodies with allowance for the primary's oblateness.

An asteroid system is a system of two or more gravitationally bound small Solar system bodies orbiting around their common centre-of-mass. We have simulated three of the most interesting asteroid systems which are best known from both ground-based and space-based surveys.

The first asteroid system among those investigated by the authors is (136617) 1994 CC, which belongs to the Apollo group of near-Earth objects. It is noteworthy for its high eccentricity, which is above 0.4 (Table 3); its orbit intersects those of the Earth and Mars. A group of researchers headed by Marina Brozovic discovered the triplicity of this asteroid based on the radar observations in 2009 (Brozovic et al., 2011). Soon after, Fang et al. (2011) presented the model of motion of the asteroid moonlets with allowance for the primary's oblateness ($J_2 = -C_{20} = 0.014 \pm 0.383$) over a time span of 300 days. $J_2 = -C_{20}$ is the second coefficient of decomposition in terms of spherical functions of the asteroid gravitational potential.

The second system among those investigated by the authors is the main-belt triple asteroid (87) Sylvia. Its first moon Romulus was discovered in 2001, and the second are Remus was discovered in 2004 (Marchis et al., 2005). Fang et al. (2012) reported the results of the implementation of the same model as that one used for the asteroid system (136617) 1994 CC, where the oblateness of the primary was also factored in ($J_2 = -C_{20} = 0.54925 \pm 0.45075$). The short-term (50 years) and long-term (1 Myr) simulations of the asteroid dynamics were performed (to determine fluctuations of the orbital elements with time and assess the stability of this three-body system).

Berthier and co-authors (Berthier et al., 2014) in their work suggested that the shape of Romulus could be elongated due to the tidal forces from the elongated and spinning primary; they supplemented the model with the primary's oblateness $J_2 = -C_{20} = 0.024^{+0.016}_{-0.009}$.

These two asteroid systems were investigated by Yu Jiang and co-authors in 2016 (Yu Jiang et al., 2016); having adopted newer data, the authors performed a numerical simulation of the orbital evolution of the moonlets in asteroid systems (136617) 1994 CC and (87) Sylvia over a time span of 550-1000 days by integrating the equations of motion using the $7^{th}/8^{th}$-order Runge-Kutta and Gauss-Jackson methods. The simulation model used in this study included mutual gravitational potential between the components and perturbations due to an irregular shape of the primary; the dynamics of the asteroid systems was investigated by considering the gravitational potential, static electric potential and magnetic potential as well.

The last asteroid system among our target ones is (136108) Haumea. It is classified as a plutoid, trans-Neptunian object and a dwarf planet. Two moons orbiting Haumea, namely Hi'iaka and Namaka, were both discovered in 2005, specific feature of these moonlets is that they both follow a retrograde orbit around the primary body. Ragozzine and Brown (Ragozzine & Brown, 2009) carried out an in-depth study of this asteroid system using precise relative astrometry from the Hubble Space Telescope and the W.M. Keck Telescope. They

calculated the oblateness of the primary ($J_2 = -C_{20} = 0.244$) and integrated the equations of motion of the asteroid system over a time span of 1260 days.

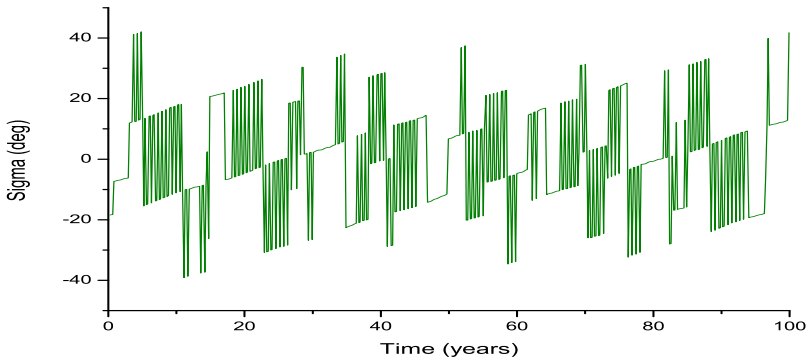

Figure 1. Changing the resonance argument σ for satellites Romulus and Remus.

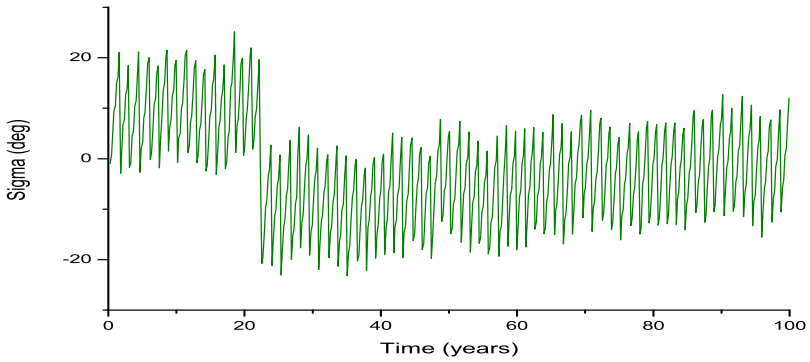

Figure 2. Changing the resonance argument σ for satellites Beta and Gamma.

2. Equation of motion

Let us consider an N-body problem according to Newton's laws of motion combined with the law of gravitation. Let the origin of the reference frame be at

the centre of the Sun and the vector $\overrightarrow{r}_j(x_j, y_j, z_j)$ define the position of the j^{th}-body with mass m_j. Thus, in the heliocentric reference frame the equation of motion appears as follows:

$$\frac{d^2\overrightarrow{r}_j}{dt^2} = -k^2(m_0 + m_j)\frac{\overrightarrow{r}_j}{r_j^3} - k^2\sum_{i=1}^{N-1} m_i\frac{\overrightarrow{r}_j - \overrightarrow{r}_i}{r_{ji}^3} -$$

$$-k^2\sum_{i=1}^{N-1} m_i\frac{\overrightarrow{r}_i}{r_i^3}, \quad i = 1..N, \quad j = 1..N, \quad i \neq j, \tag{1}$$

where k is the Gaussian gravitational constant; $\frac{d^2\overrightarrow{r}_j}{dt^2}$ is the total acceleration; $k^2(m_0 + m_j)\frac{\overrightarrow{r}_j}{r_j^3}$ is the acceleration of the j^{th}-body due to the Sun; $k^2\sum\limits_{i=1}^{N-1} m_i\frac{\overrightarrow{r}_j - \overrightarrow{r}_i}{r_{ji}^3}$ is the acceleration of the j^{th}-body due to all the other bodies in the system except for the Sun; $k^2\sum\limits_{i=1}^{N-1} m_i\frac{\overrightarrow{r}_i}{r_i^3}$ is the acceleration of the Sun due to all the other bodies in the system; are m_0 is the Solar mass.

We have adopted positions of major planets from the numerical theory DE431 (Folkner et al., 2014), because we have to take perturbations into account caused by the major planets.

Table 1. Initial conditions for the calculation of dynamical configurations of the primaries. Here, D - dimensions.

Number ast.	Mass (kg)	D (km)	C_{20}	C_{21}	C_{22}	S_{21}	S_{22}
(87)[a,b]	$1.478{\cdot}10^{19}$	385·262·232	- 0.053	0.065	0.019	0.045	0.03
(136108)[c,d]	$4.03{\cdot}10^{21}$	1960·1518·996	- 0.01	0.07	0.02	0.05	0.02
(136617)[e,f]	$2.66{\cdot}10^{11}$	0.69·0.67·0.64	- 0.013	0.083	0.001	0.08	l0.02

[a]Berthier *et al.* (2014).
[b]Fang *et al.* (2012).
[c]Ragozzine & Brown (2009).
[d]Rabinowitz *et al.* (2006).
[e]Fang *et al.* (2011).
[f]Brozovic *et al.* (2011).

2.1. Gravitational potential

If a body's shape is not-spherical, then the gravitational potential U can be easily approximated using the sum of the series. One of the options is a spherical

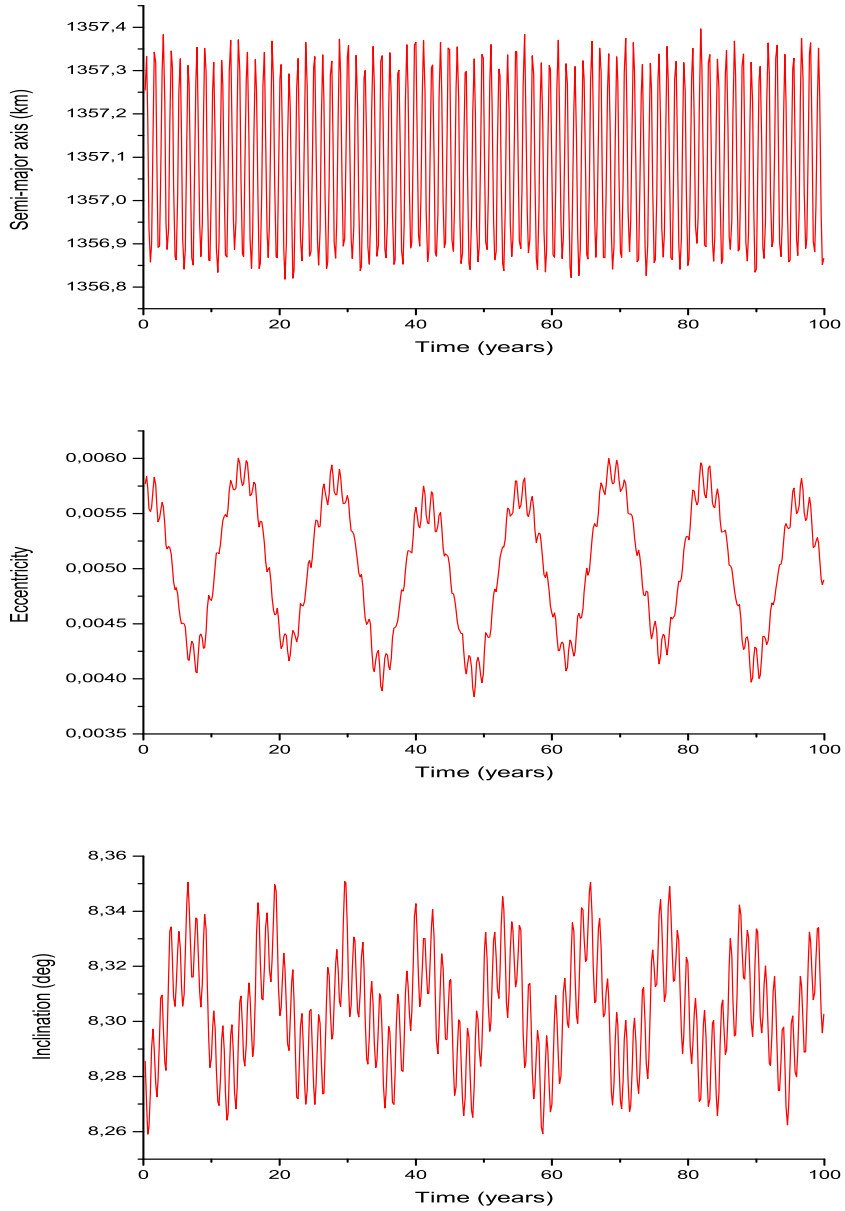

Figure 3. Numerical simulation of the orbital evolution of the moonlet Romulus: the semi-major axis, eccentricity and inclination.

Table 2. Initial conditions for the calculation of dynamical configurations of the asteroid moonlets. Here: Ga - geometric albedo; D - diameter.

Number		Moonlet 1			Moonlet 2		Ga
asteroid	Name	Mass(kg)	D (km)	Name	Mass(kg)	D (km)	
(87)[a,b,c]	Romulus	$7.915{\cdot}10^{14}$	10.8	Remus	$7.483{\cdot}10^{14}$	10.6	0.036
(136108)[d,e]	Hi'iaka	$5.1{\cdot}10^{19}$	320	Namaka	$6.37{\cdot}10^{18}$	160	0.663
(136617)[f]	Beta	$1.587{\cdot}10^{9}$	0.113	Gamma	$5.63{\cdot}10^{8}$	0.08	0.42

[a]Marchis *et al.* (2005).
[b]Fang *et al.* (2012).
[c]Masiero *et al.* (2011).
[d]Rabinowitz *et al.* (2006).
[e]Ragozzine & Brown (2009).
[f]Brozovic *et al.* (2011).

Table 3. Initial orbital parameters of the target triple asteroid systems (http://www.jpl.nasa.gov/). Here: a - semi-major axis; P - orbital period; e - eccentricity; i - inclination; Ω - long.ofascend.node; ω - arg.periapsis; M - mean anomaly.

Orbital parameters	(87) Sylvia	(136108) Haumea	(136617) 1994 CC
a (AU)	3.481808398	43.1660	1.637780212
P (years)	6.497039467	283.610	2.096001706
e	0.091145156	0.192457	0.417226647
i (deg)	10.8768036	28.191350	4.6842339
Ω *(deg)*	73.083782	121.78801	268.603487
ω *(deg)*	263.685494	240.4148	24.7567739
M (deg)	179.424861	208.1445	116.8774809
Epoch	2014 May 23	2014 May 23	2014 May 23

harmonic expansion. The usage of spherical harmonics results in a simple and handy analytical formula for the gravitational potential.

As a result from the spherical harmonic expansion, the acceleration $\overrightarrow{a}_U$ produced by the gravitational potential of an arbitrary body looks as follows (MacMillan, 1930):

$$\overrightarrow{a}_U = \overrightarrow{\nabla} U = \frac{\partial U}{\partial r}\overrightarrow{u}_r + \frac{1}{r}\frac{\partial U}{\partial \phi}\overrightarrow{u}_\phi + \frac{1}{r\cos\phi}\frac{\partial U}{\partial \lambda}\overrightarrow{u}_\lambda, \tag{2}$$

Table 4. Initial orbital parameters for the moonlets of the target triple asteroid systems. Here: a - semi-major axis; P - orbital period; e - eccentricity; i - inclination; Ω - long.ofascend.node; ω - arg.periapsis; M - mean anomaly.

Orbital	(87) Sylvia[a]		(136108) Haumea[b]		(136617) 1994 CC[c]	
parameters	Romulus	Remus	Hi'iaka	Namaka	Beta	Gamma
a (km)	1357	706.5	49880	25657	1.729	6.13
P (days)	3.6	1.4	49.5	18.3	1.2	8.4
e	0.005566	0.02721	0.0513	0.249	0.002	0.192
i (deg)	8.293	7.824	126.35	113.013	83.376	71.709
Ω *(deg)*	92.6	94.8	206.766	205.016	59.209	48.479
ω *(deg)*	61.06	357.0	154.1	178.9	130.98	96.229
M (deg)	197.0	261.0	152.8	178.5	233.699	6.07
Epoch	2004 Sep 01.0		2014 May 23		2009 Jun 12.0	

[a]Beauvalet & Marchis (2014).
[b]Ragozzine & Brown (2009).
[c]Fang *et al.* (2011).

where $\overrightarrow{u}_r$, $\overrightarrow{u}_\phi$, $\overrightarrow{u}_\lambda$ are the unit vectors in the r, ϕ, λ basis;

$$U = \frac{k^2}{r} \sum_{l=0}^{\infty} \left(\frac{a_e}{r}\right)^l \sum_{n=0}^{l} P_{l,n}(\sin\phi) \left[C_{l,n} \cos n\lambda + S_{l,n} \sin n\lambda\right], \tag{3}$$

where a_e is the mean equatorial radius of the attracting arbitrary body; $C_{l,n}$ and $S_{l,n}$ are the coefficients of expansion of the attracting body gravitational field; r, ϕ and λ are the coordinates in the spherical reference frame of the attracting body; and $P_{l,n}$ are the associated Legendre functions.

The coefficients $C_{l,n}$ and $S_{l,n}$ depend on the body's shape and mass distribution within that body; the coefficients are dimensionless. There are numerous coefficients of the expansion calculated for the major planets, the Sun and the Moon; for instance, the spherical harmonic model of the gravitational potential of the Earth - EGM-2008 and Moon - LP-1201. In our model, we only used coefficients C_{20} for the aforementioned objects due to their far distance from the primary as compared to the distance from the moonlets; the other coefficients are negligible. It seems reasonable to use a higher order spherical harmonic expansion of the gravitational field for close approaches to planets or their moons.

When simulating the gravitational field of an asteroid, a small Solar System body, we bee-can have adopted two approximations: the density ρ is constant throughout the asteroid and the asteroid has a three-axial ellipsoid shape with the semi-axes a, b and c.

Consider the coefficients $C_{l,n}$ and $S_{l,n}$ of the asteroid from (Troianskyi, 2015). As the origin of the reference frame is at the centre of the body, the

Table 5. Periods of variations in the Keplerian orbital elements orbits of the asteroid moonlets (in years).

Number	(87) Sylvia		(136108) Haumea		(136617) 1994 CC	
periods	Romulus	Remus	Hi'iaka	Namaka	Beta	Gamma
Period 1: a	1.234	8.007	25.019	25.019	0.872	4.259
Period 2: a	0.225	0.609	0.458	1.118	–	0.411
Period 3: a	0.165	0.276	0.325	0.443	–	–
Period 4: a	0.103	–	–	–	–	–
Period 1: e	13.710	0.609	>100	>100	0.380	>100
Period 2: e	0.193	0.276	1.168	9.099	–	21.293
Period 3: e	–	0.145	–	0.441	–	4.259
Period 4: e	–	0.113	–	–	–	1.599
Period 5: e	–	–	–	–	–	0.455
Period 1: i	11.638	7.944	18.883	18.883	20.137	20.016
Period 2: i	1.287	1.287	0.192	0.192	–	–
Period 3: i	0.223	0.223	–	–	–	–
Period 4: i	0.193	0.195	–	–	–	–
Period 1: ω	5.923	6.903	0.380	0.381	10.110	20.424
Period 2: ω	0.196	0.586	0.190	0.190	5.048	1.599
Period 3: ω	–	0.293	–	–	3.367	–
Period 1: Ω	11.638	1.159	18.883	18.883	16.407	0.190
Period 2: Ω	0.193	0.579	0.188	0.188	–	–
Period 3: Ω	–	0.386	–	–	–	–
Period 4: Ω	–	0.283	–	–	–	–

first coefficients of the gravitational field expansion are zero. If $l = 2$ and $n = 0$, $n = 1$ and $n = 2$, then the following equations are obtained (Murray & Dermot, 2000):

$$\begin{cases} C_{20} = \frac{2C-(A+B)}{2m_A a_e^2}, \\ C_{21} = \frac{E}{m_A a_e^2}, \\ C_{22} = \frac{B-A}{4m_A a_e^2}, \end{cases} \qquad \begin{cases} S_{21} = \frac{D}{m_A a_e^2}, \\ S_{22} = \frac{F}{2m_A a_e^2}, \end{cases} \tag{4}$$

where A, B and C are the axial moments of inertia; D, E and F are the cen-

Table 6. The relationship between the orbital periods and periods of variations in the Keplerian orbital elements (in years).

(87) Sylvia	(136108) Haumea	(136617) 1994 CC
Romulus	Hi'iaka	Beta
$P1_a$·48-$P_{Jupiter}$·5=-0.064	$P1_a$·34-P_{Haumea}·3=-0.19	$P1_a$·8-P_{Earth}·7=-0.027
$P2_a$·1-$P_{Romulus}$·23=-0.001	$P2_a$·3-$P_{Hi'iaka}$·10=0.02	–
$P3_a$·1-$P_{Romulus}$·17=-0.003	$P3_a$·5-$P_{Hi'iaka}$·12=-0.001	–
$P4_a$·1-$P_{Romulus}$·10=0.004	–	–
$P1_e$·9-P_{Sylvia}·19=-0.050	$P1_e$·2-P_{Haumea}·1=0	$P1_e$·5-P_{Mars}·1=0.019
$P2_e$·1-$P_{Romulus}$·20=-0.004	$P2_e$·1-$P_{Hi'iaka}$·9=-0.05	–
$P1_i$·24-P_{Sylvia}·43=-0.056	$P1_i$·15-P_{Haumea}·1=-0.36	$P1_i$·5-P_{1994CC}·48=0.076
$P2_i$·5-P_{Sylvia}·1=-0.064	$P2_i$·2-$P_{Hi'iaka}$·3=-0.02	–
$P3_i$·1-$P_{Romulus}$·23=-0.0035	–	–
$P4_i$·1-$P_{Romulus}$·20=-0.004	–	–
$P1_\omega$·2-$P_{Jupiter}$·1=-0.016	$P1_\omega$·1-$P_{Hi'iaka}$·3=-0.03	$P1_\omega$·8-P_{Mars}·43=0.006
$P2_\omega$ ·1-$P_{Romulus}$·20=-0.001	$P2_\omega$·2-$P_{Hi'iaka}$·3=-0.03	$P2_\omega$·1-P_{Earth}·5=0.048
–	–	$P3_\omega$·5-P_{1994CC}·8=0.066
$P1_\Omega$·24-P_{Sylvia}·43=-0.056	$P1_\Omega$·15-P_{Haumea}·1=-0.36	$P1_\Omega$ ·6-P_{1994CC}·47=-0.069
$P2_\Omega$ ·1-$P_{Romulus}$·20=-0.004	$P2_\Omega$·3-$P_{Hi'iaka}$·4=-0.02	–
(87) Sylvia	(136108) Haumea	(136617) 1994 CC
Remus	Namaka	Gamma
$P1_a$·40-$P_{Jupiter}$·27=0.026	$P1_a$·34-P_{Haumea}·3=-0.19	$P1_a$·1-P_{1994CC}·2=0.067
$P2_a$·32-P_{Sylvia}·3=-0.007	$P2_a$·1-P_{Namaka}·22=0.02	$P2_a$·5-P_{1994CC}·1=-0.042
$P3_a$·43-$P_{Jupiter}$·1=0.025	$P3_a$·1-P_{Namaka}·9=-0.01	–
$P1_e$·32-P_{Sylvia}·3=-0.007	$P1_e$·2-P_{Haumea}·1=0	–
$P2_e$·43-$P_{Jupiter}$·1=0.025	$P2_e$·163-$P_{Neptune}$·9=0.09	$P2_e$·3-P_{Mars}·34=-0.068
$P3_e$·1-P_{Remus}·38=-0.001	$P3_e$·1-P_{Namaka}·9=-0.01	$P3_e$·1-P_{1994CC}·2=0.067
$P4_e$·1-P_{Remus}·29=0.002	–	$P4_e$·5-P_{Earth}·8=-0.005
–	–	$P5_e$·2-P_{Earth}·1=-0.091
$P1_i$·9-P_{Sylvia}·11=0.027	$P1_i$·15-P_{Haumea}·1=-0.36	$P1_i$·1-P_{Earth}·20=0.016
$P2_i$·5-P_{Sylvia}·1=-0.064	$P2_i$·1-P_{Namaka}·4=-0.01	–
$P3_i$·29-P_{Sylvia}·1=-0.026	–	–
$P4_i$·33-P_{Sylvia}·1=-0.069	–	–
$P1_\omega$·16-P_{Sylvia}·17=-0.002	$P1_\omega$·1-P_{Namaka}·8=-0.02	$P1_\omega$·4-P_{1994CC}·39=-0.046
$P2_\omega$·11-P_{Sylvia}·1=-0.047	$P2_\omega$·1-P_{Namaka}·4=-0.01	$P2_\omega$·5-P_{Earth}·8=0.005
$P3_\omega$·22-P_{Sylvia}·1=-0.047	–	–
$P1_\Omega$·28-P_{Sylvia}·5=-0.046	$P1_\Omega$·15-P_{Haumea}·1=-0.36	$P1_\Omega$·1-P_{Gamma}·8=0.006
$P2_\Omega$·41-$P_{Jupiter}$·2=0.027	$P2_\Omega$·37-P_{Namaka}·4=-0.01	–
$P3_\Omega$·17-P_{Sylvia}·1=0.068	–	–
$P4_\Omega$·23-P_{Sylvia}·1=0.012	–	–

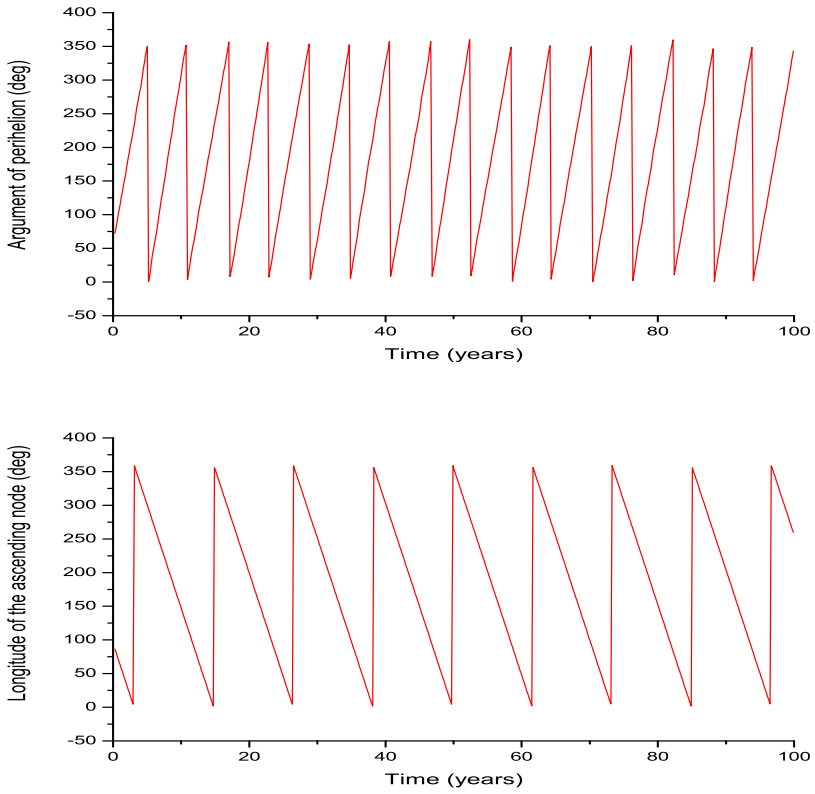

Figure 4. Numerical simulation of the orbital evolution of the moonlet Romulus: the argument of perihelion and the longitude of the ascending node.

trifugal moments of inertia and m_A is the asteroid mass.

$$\begin{cases} A = \int (b^2 + c^2) dm_A = \frac{1}{3}\rho(b^3 ac + c^3 ab), \\ B = \int (a^2 + c^2) dm_A = \frac{1}{3}\rho(a^3 bc + c^3 ab), \\ C = \int (a^2 + b^2) dm_A = \frac{1}{3}\rho(a^3 bc + b^3 ac), \\ \\ D = \int (bc) dm_A = \frac{1}{4}\rho ab^2 c^2, \\ E = \int (ac) dm_A = \frac{1}{4}\rho a^2 bc^2, \\ F = \int (ab) dm_A = \frac{1}{4}\rho a^2 b^2 c. \end{cases} \tag{5}$$

Changes in the Keplerian orbital elements from this effect are described by the authors in an earlier work (Troianskyi, 2015).

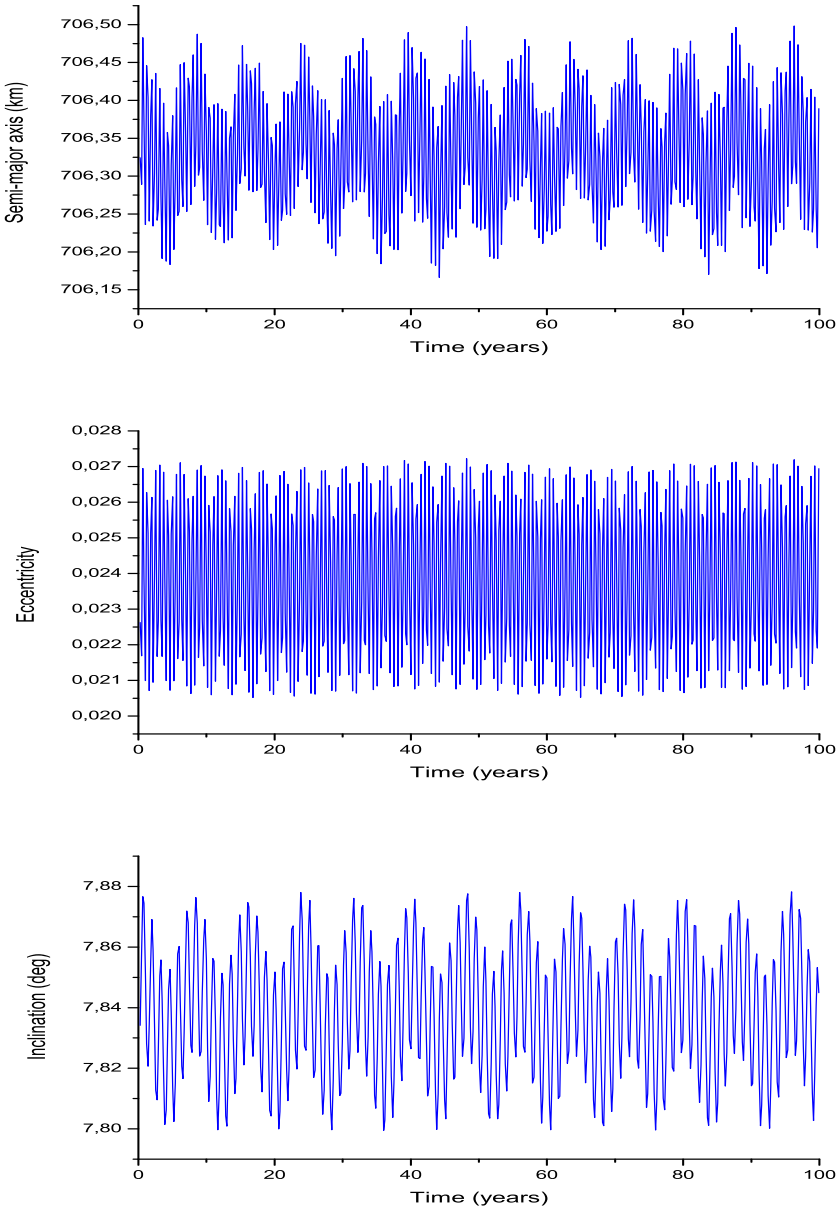

Figure 5. Numerical simulation of the orbital evolution of the moonlet Remus: the semi-major axis, eccentricity and inclination.

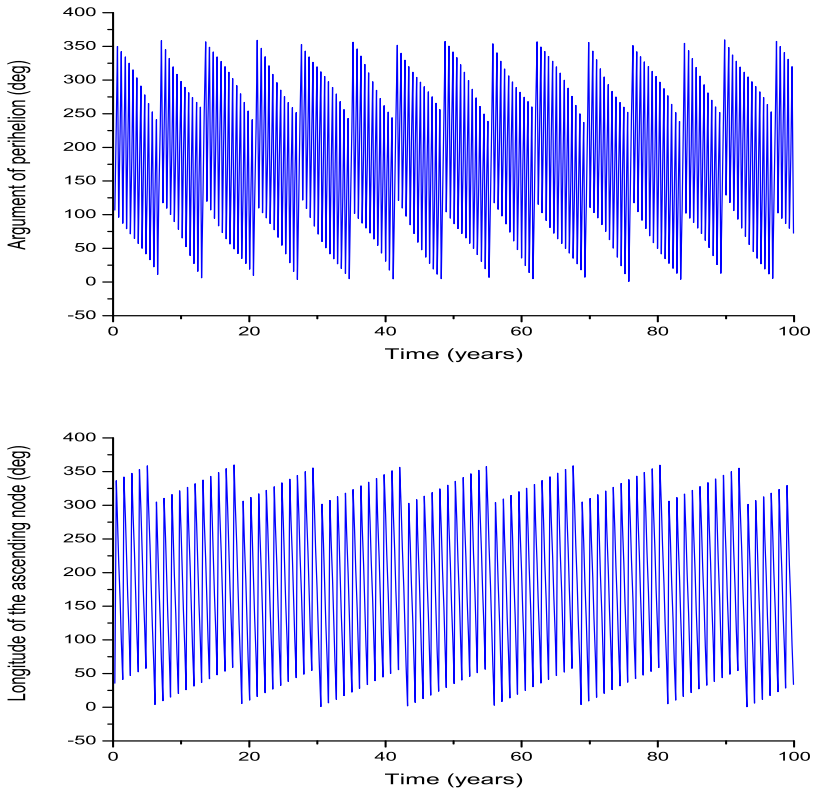

Figure 6. Numerical simulation of the orbital evolution of the moonlet Remus: the argument of perihelion and the longitude of the ascending node.

2.2. Perturbations due to the tidal deformation of the primary components

As a result of the gravitational attraction of an asteroid moonlet, every element of the primary is exposed to the gravitational force which causes tidal deformation of the primary. Due to this deformation the asteroid gravity changes, which results in the emergence of additional forces with additional gravitational potential:

$$\overrightarrow{a}_{Tide} = \frac{Gm_{st}a_e^5}{\overrightarrow{r}_{ASt}^6} P_2(\cos\theta), \tag{6}$$

where m_{St} is the mass of the asteroid's moon; $\overrightarrow{r}_{ASt}$ is the vector of the moon's position relative to the asteroid and θ is the angle between direction on the

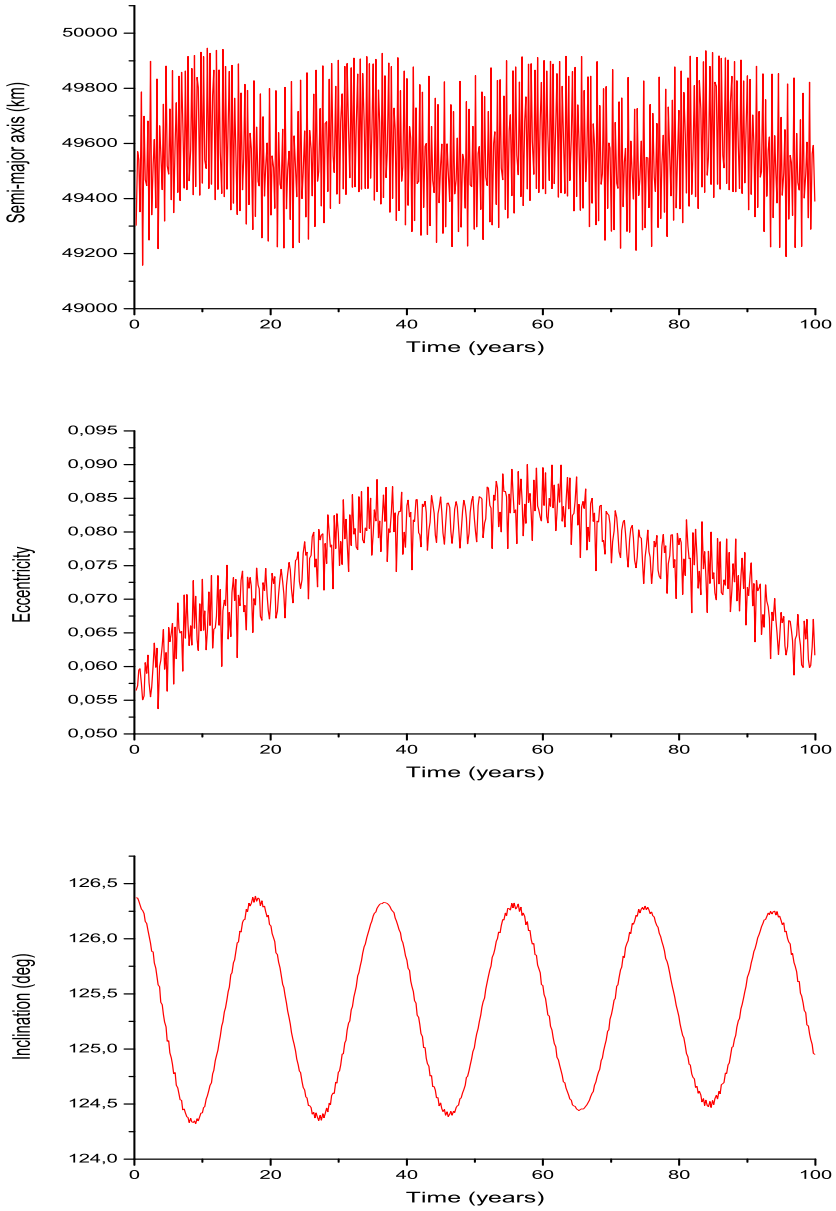

Figure 7. Numerical simulation of the orbital evolution of the moonlet Hi'iaka: the semi-major axis, eccentricity and inclination.

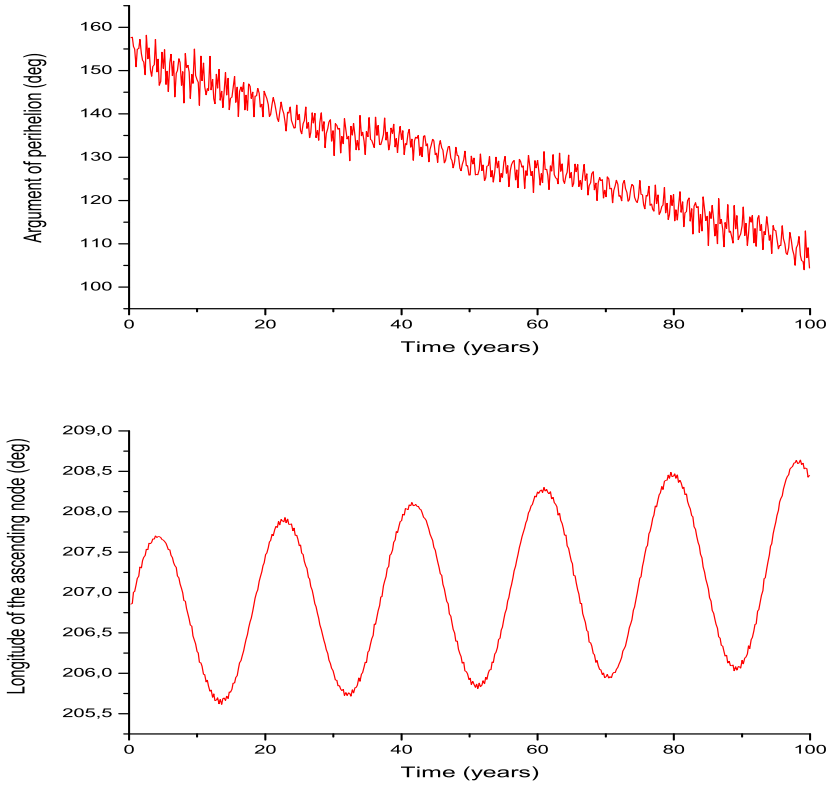

Figure 8. Numerical simulation of the orbital evolution of the moonlet Hi'iaka: the argument of perihelion and the longitude of the ascending node.

satellite and the tidal hump. In our case, the angle $\theta = 0^o$, which results in $\cos\theta = 1 \Rightarrow P_2(\cos\theta) = 1$; then, equation (6) can be written as follows:

$$\overrightarrow{a}_{Tide} = \frac{Gm_{St}a_e^5}{\overrightarrow{r}_{ASt}^6}. \tag{7}$$

2.3. Perturbations due to the effect of solar radiation pressure

In the theory of motion of asteroid moons, the solar radiation pressure exerted upon their surfaces should also be taken into account. To this end, we have used decomposition of the solar radiation pressure induced acceleration a_{Lp}

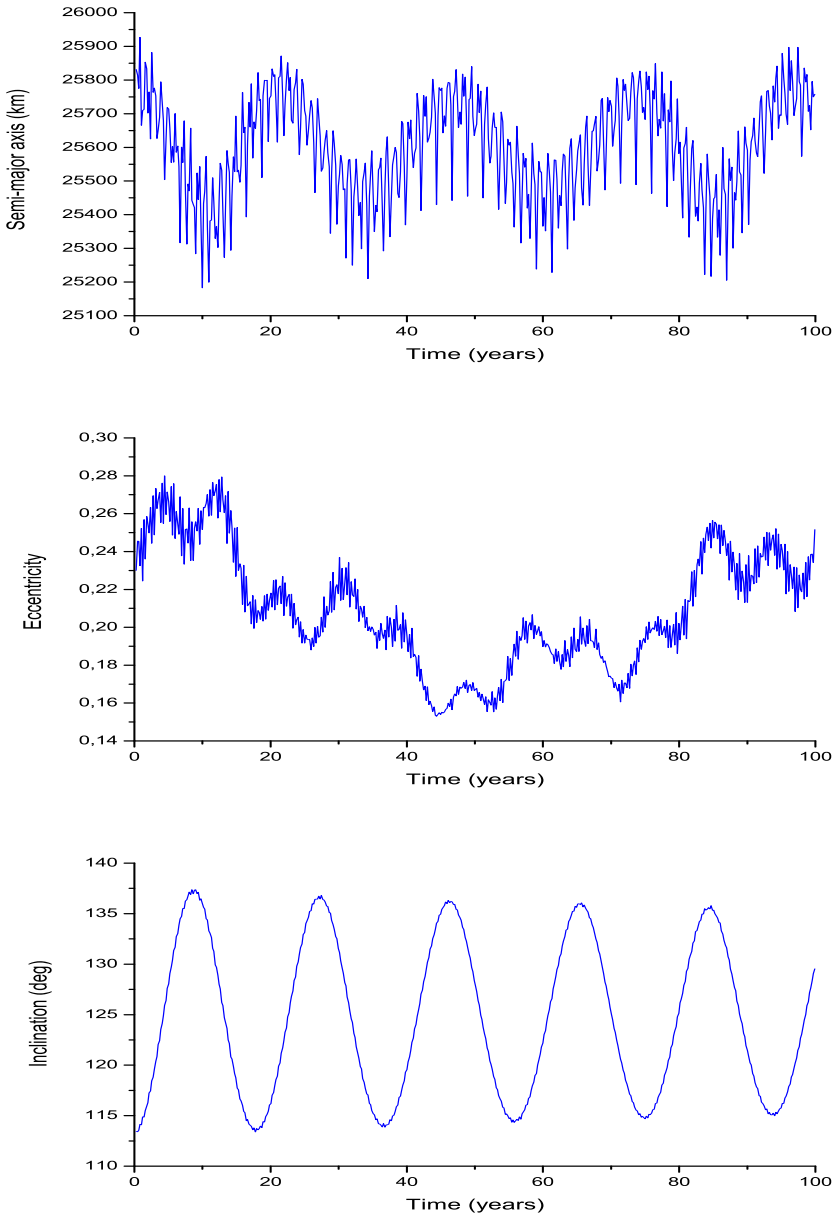

Figure 9. Numerical simulation of the orbital evolution of the moonlet Namaka: the semi-major axis, eccentricity and inclination.

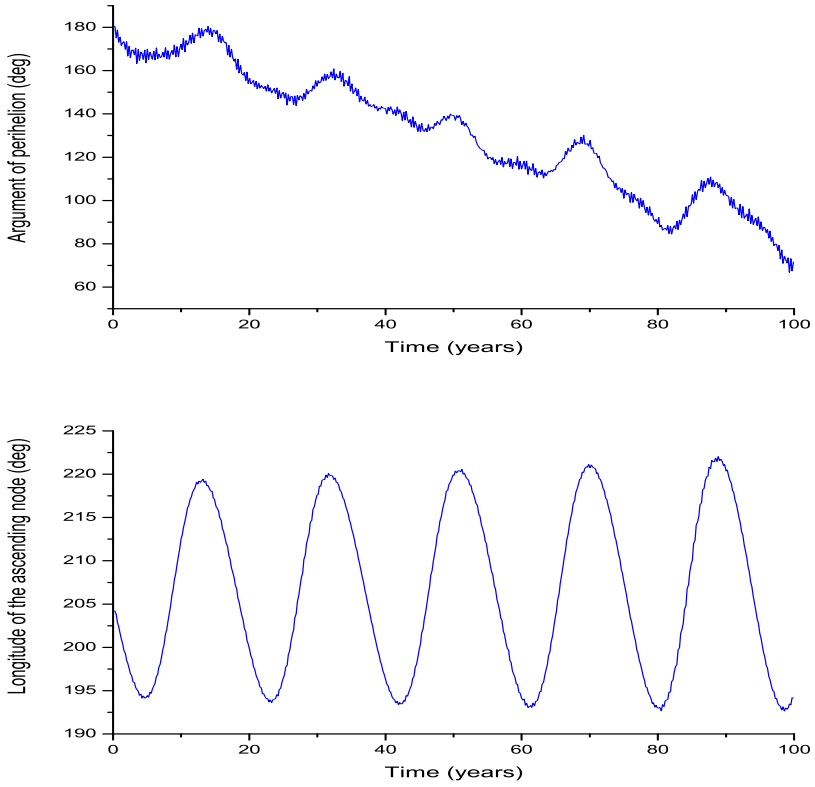

Figure 10. Numerical simulation of the orbital evolution of the moonlet Namaka: the argument of perihelion and the longitude of the ascending node.

(Martyusheva et al., 2015):

$$\overrightarrow{a}_{Lp} = \left(1 + \frac{4}{9}\delta\right) q \frac{S}{m_{St}} \Psi \left(\frac{r_A}{|\overrightarrow{r}_{St}|}\right) \frac{\overrightarrow{r}_{St}}{|\overrightarrow{r}_{St}|}, \tag{8}$$

where δ is the geometric albedo; $q = 4.5605 \cdot 10^{-6}\,\mathrm{N\,m^{-2}}$ is the solar constant; S is the cross-sectional area of the asteroid moon; Ψ is the shadow function which will be discussed in detail below; r_A is the distance between the asteroid and the Sun and $\overrightarrow{r}_{St}$ is the vector of the asteroid moon position relative to the Sun.

Changes in the Keplerian orbital elements from this effect are described by the authors in an earlier work (Troianskyi & Bazyey, 2015).

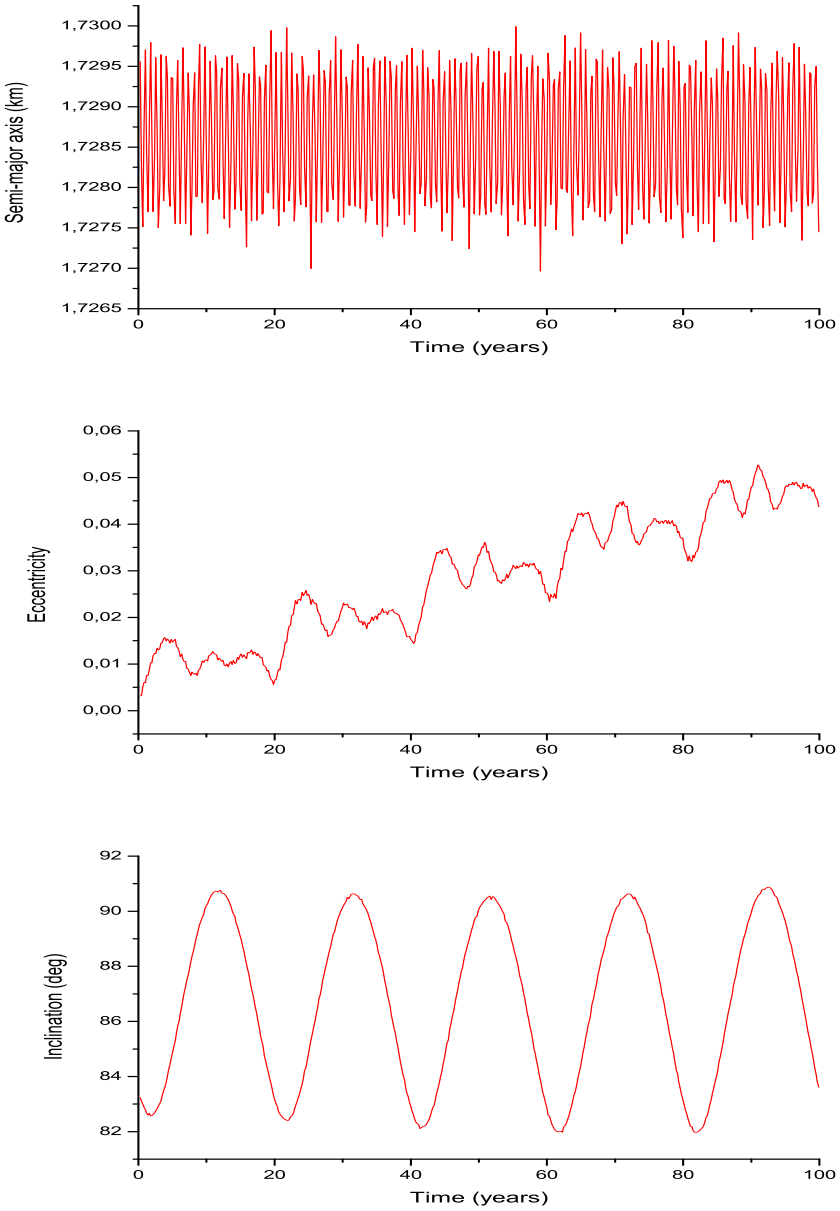

Figure 11. Numerical simulation of the orbital evolution of the moonlet Beta: the semi-major axis, eccentricity and inclination.

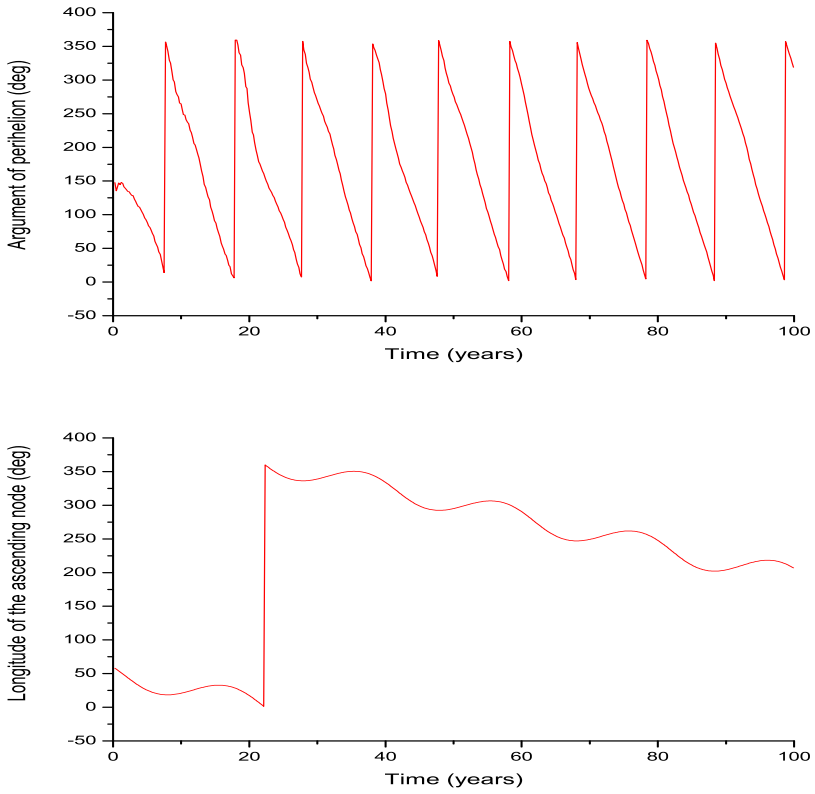

Figure 12. Numerical simulation of the orbital evolution of the moonlet Beta: the argument of perihelion and the longitude of the ascending node.

2.4. Shadow function

Equation (8) includes a shadow function. Let us examine in more detail how this function is calculated in our model. Ferraz-Mello introduced the term shadow function Ψ (Ferraz-Mello, 1972). This function is equal to 1 when the asteroid's moon is illuminated by the Sun, and it is equal to zero when it is in shadow. To a first approximation the shadow is reckoned to be cylindrical in shape.

In our model the shadow is supposed to be cone-shaped (Troianskyi & Bazyey, 2015), which enables to more accurately determine the instants of the asteroid moon entries into and exits from the shadow. Thus, the shadow function

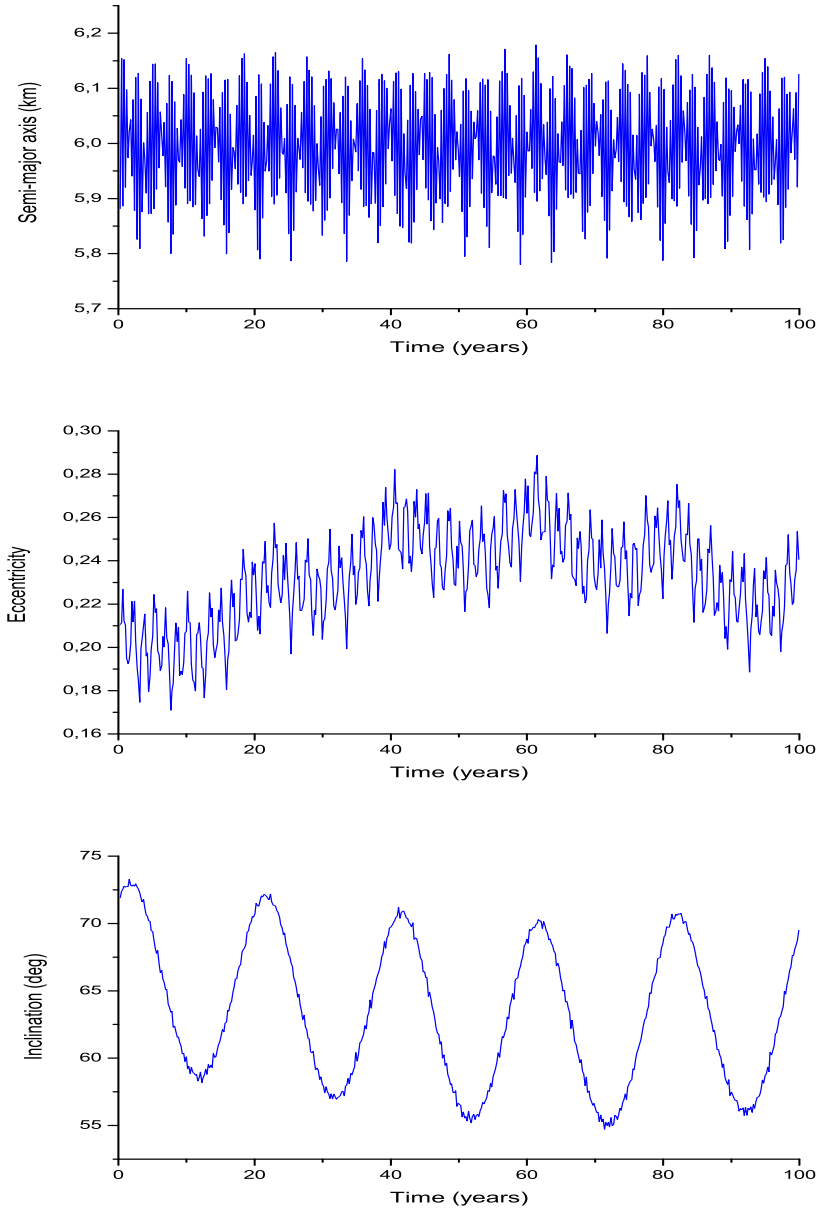

Figure 13. Numerical simulation of the orbital evolution of the moonlet Gamma: the semi-major axis, eccentricity and inclination.

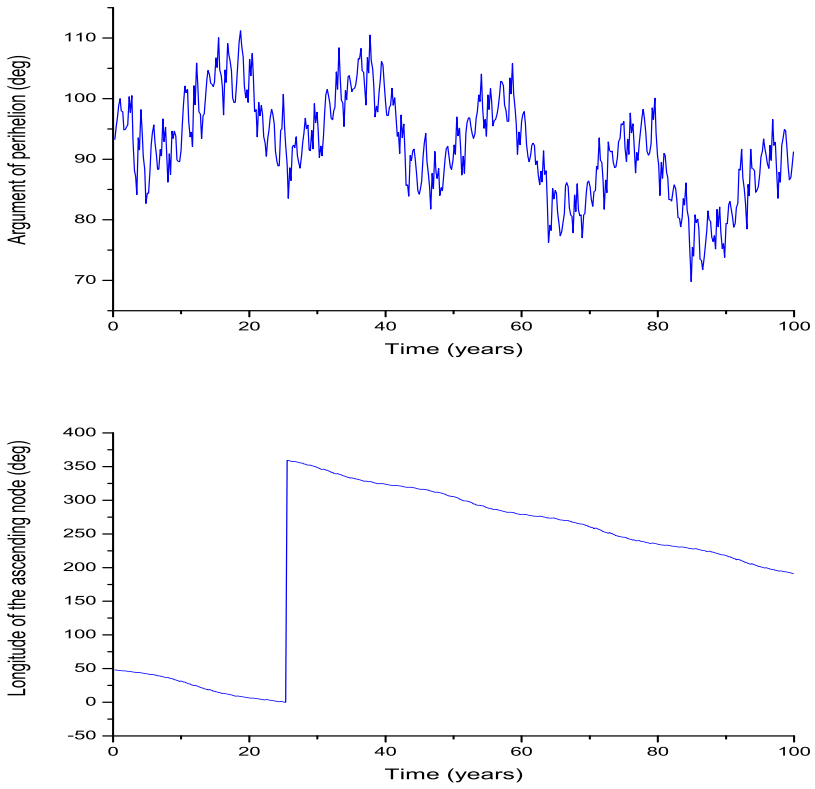

Figure 14. Numerical simulation of the orbital evolution of the moonlet Gamma: the argument of perihelion and the longitude of the ascending node.

for the cone-shaped shadow looks as follows:

$$\Psi = \begin{cases} 0, & \text{if} \quad \frac{x_{St}^2}{a_c^2} + \frac{y_{St}^2}{b_c^2} - \frac{z_{St}^2}{c_c^2} = 0, \\ 1, & \text{if} \quad \frac{x_{St}^2}{a_c^2} + \frac{y_{St}^2}{b_c^2} - \frac{z_{St}^2}{c_c^2} = 1, \end{cases} \tag{9}$$

where a_c, b_c, c_c are the axes of the shadow cone; x_{St}, y_{St}, z_{St} are the asteroid moons coordinates in the asteroid-centric Cartesian coordinate frame.

The model can also factor in variations in the size and shape of the shadow projected onto the asteroid.

2.5. Numerical integration of equations of motion

We have integrated equation of motion (1) with allowance for the non-sphericity of the attracting bodies and the effect of solar radiation pressure on the asteroid moons in the Cartesian coordinate frame.

The Everhart method (Everhart, 1974) is currently the standard method for the numerical integration in celestial mechanics. We have used the Everhart 15^{th}- order method (Bazyey & Kara, 2009) for the numerical integration of the equations of motion.

When numerically integrating equations of motion, the verification of the model or the so-called integration step size control must be performed. The verified solution of our numerical model, which does not exceed 10^{-6} m, has been obtained by the methods of double step-size forward-backward integration of the equations of motion over a time span of 100 years with a time step of 30 seconds.

Using the conservation-of-energy law, we can set down the following: in a closed-loop N-body system the sum of kinetic (T) and potential (U) energies is constant

$$T - U = \text{const}; \tag{10}$$

then, we can use this condition as a criterion of the numerical model stability. For ease of use, let us write down the equation as follows:

$$\frac{1}{2}\sum_{i=1}^{N} m_i \left[\left(x_i^{'} - \frac{\sum\limits_{i=1}^{N} m_i x_i^{'}}{M} \right)^2 + \left(y_i^{'} - \frac{\sum\limits_{i=1}^{N} m_i y_i^{'}}{M} \right)^2 + \left(z_i^{'} - \frac{\sum\limits_{i=1}^{N} m_i z_i^{'}}{M} \right)^2 \right] -$$

$$-G\sum_{i=1}^{N}\sum_{j=1}^{N} \frac{m_i m_j}{r_{ij}} = \text{const}, \tag{11}$$

where $M = \sum\limits_{i=1}^{N} m_i$ and $i \neq j$.

3. Verification and validation of the model

There were almost 330 asteroids and trans-Neptunian objects with two or more discovered moons known at the moment of writing this paper (http://www.johnstonsarchive.net/astro/asteroidmoons.html). We have selected (136617) 1994 CC, (87) Sylvia and (136108) Haumea, which are triple asteroid systems; all six independent Keplerian orbital elements (Table 2), as well as masses and diameters (Table 4) of the moons in these asteroid systems determined with reasonable accuracy, are available to date.

At first, applying initial conditions to one of the primaries (Tables 1 and Tables 3) we compute its heliocentric coordinate. Then, we go to the asteroid-centric reference frame to examine the motion of asteroid moons there, with considering earlier described indignation (Sections 2.1-2.4).

Figs. 3-14 show the plotted variations in the selected orbital elements, such as the semi-major axis, eccentricity, inclination, argument of perihelion and the longitude of ascending node, for the target asteroid systems. The numerical simulations of the orbital evolution for the asteroid moonlets Romulus, Remus, Hi'iaka, Namaka, Beta and Gamma are presented in Figs. 1-6, respectively.

3.1. Periodogram analysis

Periodic variations have been detected in all orbital elements. The main periods of orbital variations (Table 5) have been computed using the MCV software package (Andronov & Baklanov, 2004).

The periods of some orbital-element variations of the moonlets within each asteroid system are very similar, which may be due to the exposure to one and the same effect; hence, the moonlets in the asteroid systems (136617) 1994 CC and (87) Sylvia are in orbital resonance (Troianskyi, 2016), while those in (136108) Haumea are approaching it.

Table 6 presents the relationship between the variations in the Keplerian orbital elements and barycentric orbital periods of the asteroid systems (given in Table 3), asteroid moonlets (given in Table 4) and the closest major planets, namely the Earth (365.256 days), Mars (686.980 days). Jupiter (4332.589 days) and Neptune (60189.0 days) (http://nssdc.gsfc.nasa.gov/planetary/factsheet/). We found out that the periods of variations in the Keplerian orbital elements, for which the relationship with the barycentric orbital periods of the asteroid systems can be expressed as small integers, result from the approach to the Sun when following elliptical orbits. Those periods of variations in the Keplerian orbital elements, for which the relationship with the orbital periods of the asteroid moonlets can be expressed as small integers, result from the approach of the moons to the non-symmetric primary body when following elliptical orbits. Those periods of variations in the Keplerian orbital elements, for which the relationship with the orbital periods of the closest major planets can be expressed as small integers, result from the periodic approaches to these planets.

As it was mentioned above, some periods of the variations of the Keplerian orbital elements of the asteroid moonlets are similar, which may be due to the exposure to one and the same effect; the causes of such similarity can be deduced from Table 6. In the asteroid system (87) Sylvia, for the moonlet Romulus $\mathrm{Period}\,2_e \approx \mathrm{Period}\,2_\omega$, which is the result of its orbital motion; $\mathrm{Period}\,1_i \approx \mathrm{Period}\,1_\Omega$ is the result of the simulated orbital motion of the asteroid system (87) Sylvia, while $\mathrm{Period}\,2_a \approx \mathrm{Period}\,1_e$ is the same as for the moonlet Remus; and the relationship $\mathrm{Period}\,3_a \approx \mathrm{Period}\,2_e$ resulted from the periodic approaches to Jupiter. The variations of the orbital inclinations for

both asteroid moonlets have equal periods $\mathrm{Period}\,2_i$, $\mathrm{Period}\,3_i$ and $\mathrm{Period}\,4_i$. $\mathrm{Period}\,2_i$ resulted from the orbital motion of the asteroid system, while the other periods of variations are correlated to the orbital motion of its moonlets. The moons in the asteroid system (136108) Haumea show noticeable variations with long and short periods, and as it can be seen from Table 5, there are equal periods of variations in each Keplerian element of these moons. $\mathrm{Period}\,1_a$, $\mathrm{Period}\,1_e$, $\mathrm{Period}\,1_i$ and $\mathrm{Period}\,1_\Omega$ correspond to the variations with long periods due to the orbital motion of the asteroid system (136108) Haumea. The identical $\mathrm{Period}\,2_i, \mathrm{Period}\,1_\omega, \mathrm{Period}\,2_\omega$ and $\mathrm{Period}\,2_\Omega$ correspond to the short-period variations in the Keplerian orbital elements which depend on the orbital motion of the asteroid moons. In the asteroid system (136617) 1994 CC, such similarity of the variations in the Keplerian orbital elements have only been found for the moon Gamma: $\mathrm{Period}\,1_a \approx \mathrm{Period}\,3_e$ resulted from the orbital motion of the asteroid system (136617) 1994 CC, while $\mathrm{Period}\,4_e \approx \mathrm{Period}\,2_\omega$ is due to the periodic approaches to the Earth.

A different number of similarities of variations in the Keplerian orbital elements of the moonlets in different asteroid systems can be associated with their position in the Solar system. In (87) Sylvia and (136617) 1994 CC there are more perturbations emerged by the motion of the moons as compared to those in (136108) Haumea.

We also detected secular variations in the argument of perihelion and the longitude of ascending node for the moonlets Romulus and Remus; in the argument of perihelion for the moonlets Hiiaka and Namaka; in the eccentricity, argument of perihelion and the longitude of ascending node for the moonlet Beta; and in the inclination, argument of perihelion and the longitude of ascending node for the moonlet Gamma.

As a consequence, we can see variations in the Keplerian orbital elements (Table 5), which are typical for all bodies in the Solar system. Secular variations in the major planets are already known (Murray & Dermot, 2000); and a similar pattern can be seen in the asteroid systems-there are secular variations, variations of mid-term duration and those with shorter periods due to relatively smaller masses of these asteroid systems. These are compared to the major planets.

3.2. Resonances in asteroid systems

One of the authors calculated resonances in asteroid systems in their earlier work (Troianskyi, 2016).

For (87) Sylvia and (136617) 1994 CC, calculated orbital resonance between their moons is given by equations (12). If the orbital periods of two moons of an asteroid are related by a ratio of small integers, such moons are in orbital resonance.

$$\begin{aligned} 3 \cdot P_{Romulus} - 8 \cdot P_{Remus} &\approx 0, \\ 7 \cdot P_{Beta} - 1 \cdot P_{Gamma} &\approx 0. \end{aligned} \tag{12}$$

The fact that satellites an in resonance indicates that the system was formed over a long time.

To give the proof, one has to calculate the so-called resonance angle or resonance argument σ, which equals (Murray & Dermot, 2000):

$$\sigma = n_1 \cdot \lambda_2 - n_2 \cdot \lambda_1 + (n_2 - n_1) \cdot L_1, \tag{13}$$

where n_1 and n_2 are integers (appearing also in Eq.(12)), λ_1 and λ_2 are mean longitudes of the first and second moons, respectively, and L_1 is the longitude of pericenter of the first moon.

$$\lambda = M + \omega, \tag{14}$$

where M is anomaly, ω is the argument of pericenter (Table 4).

$$L_1 = \omega_1 + \Omega_1, \tag{15}$$

where ω_1 and Ω_1 are the argument of pericenter and longitude of ascending node (Table 4), respectively, of the first moon.

The angle σ varies, over a long period, in an interval smaller than 360 degrees for Romulus and Remus (Figure 1) and Beta and Gamma (Figure 2). It means that the Romulus is in 8:3 mean-motion resonance with the Remus and Beta is in 1:7 mean-motion resonance with the Gamma (this is the proof of the existence of resonance).

4. Conclusion

A numerical simulation model for the investigation of specific features of the orbital evolution of binary and multiple small-Solar-system-body systems which accounts for the force of gravitational attraction of the Sun and major planets, non-sphericity of the model components, as well as solar radiation pressure with allowance for the shadow function, has been developed.

The verification and validation of the simulation model have been performed for the asteroid systems (136617) 1994 CC and (87) Sylvia. The variations in the Keplerian orbital elements obtained over a time span of 100 years do not contradict those reported by other studies. Secular variations in some Keplerian orbital elements of the asteroid moons have been found. The values of periodic variations for all orbital elements have been calculated and their causes have been shown. Identical periodic variations in the Keplerian orbital elements of one and the same asteroid moon have also been detected.

The first five expansions of the gravitational field (C_{20}, C_{21}, C_{22}, S_{21}, S_{22}) have been calculated for the primary bodies in the asteroid systems (Table 1). Not all the values obtained are consistent with the earlier results of other authors, which may be due to the difference in the initial parameters (the authors of the article use newer data) and in the methods and techniques for their determination (the authors of the article take more gravitational and non-gravitational corrections in the theory of motion).

References

Aarseth, J. Sverre: 2003, *Gravitational N-Body Simulations*, Cambridge, University press.

Andronov, I.L., Baklanov, A.V.: 2004, *AstSR,* **5**, 264

Bazyey, A.A., Kara, I.V.: 2009, *AstSR,* **6(2)**, 155

Beauvalet, L., and Marchis, F.: 2014, *Icarus,* **241**, 13

Berthier, J., Vachier, F., Marchis, F., Durech, J., Carry, B.: 2014, *Icarus,* **239**, 118

Brozovic, Marina, Benner, Lance A.M., Taylor, Patrick A., Nolan, Michael C., Howell, Ellen S., Magri, Christopher, Scheeres, Daniel J., Giorgini, Jon D., Pollock, Joseph T., Pravec, Petr, Galad, Adrian, Fang, Julia, Margot, Jean-Luc, Busch, Michael W., Shepard, Michael K., Reichart, Daniel E., Ivarsen, Kevin M., Haislip, Joshua B., LaCluyze, Aaron P., Jao, Joseph, Slade, Martin A., Lawrence, Kenneth J., Hicks, Michael D.: 2011, *Icarus,* **216**, 241

Everhart, E.: 1974, *Celest. Mech.,* **10**, 35

Fang, J., Margot, J.-L., Rojo, P.: 2012, *Astron. J.,* **144**, 70

Fang J., J.-L. Margot, M. Brozovic, M. C. Nolan, L. A. M. Benner, and P. A. Taylor: 2011, *Astron. J.,* **141**, 154

Ferraz-Mello S.: 1972, *Celest. Mech.,* **5**, 80

Folkner, W.M., Williams, J.G., Boggs, D.H., Park, R.S., Kuchynka, P.: 2014, *The Interplanetary Network Progress Report,* **42-196**, 1

MacMillan, W.D.: 1930, *The Theory of the Potential*, Dover Press,

Marchis, F., Descamps, P., Baek, M., Harris, A. W., Kaasalainen, M., Berthier, J., Hestroffer, D. , Vachier, F.: 2008, *Icarus* **196**, 97

Marchis, F., Descamps, P., Hestroffer, D., Berthier, J.: 2005, *Nature,* **436**, 822

Martyusheva, A., Petrov, N., Polyakhova, E.N.: 2015, *Messenger of St. Petersburg University* **2(60)**, 135

Masiero, Joseph R., Mainzer, A.K., Grav, T., Bauer, J.M., Cutri, R.M., Dailey, J., Eisenhardt, P.R.M., McMillan, R.S., Spahr, T.B., Skrutskie, M.F., Tholen, D., Walker, R.G., Wright, E.L., DeBaun, E., Elsbury, D., Gautier, T., Gomillion, S., Wilkins, A.: 2011, *Astrophys. J.,* **741**, 68

Murray, C.D., Dermot, S.F.: 2000, *Solar System Dynamics*, Cambridge, University press.

Rabinowitz, D. L., Barkume, K., Brown, M.E., Roe, H., Schwartz, M., Tourtellotte, S., Trujillo, C.: 2006, *Astron. J.,* **639**, 1238

Ragozzine, D., Brown, M.E.: 2009, *Astron. J.,* **137**, 4766

Troianskyi V.V.: 2015, *Odessa Astronomical Publ.,* **28(2)**, 299

Troianskyi V.V.: 2016, *Odessa Astronomical Publ.,* **29**, 221

Troianskyi V.V., Bazyey O.A.: 2015, *Odessa Astronomical Publ.,* **28(1)**, 76

Yu Jiang, Yun Zhang, Hexi Baoyin, Li Junfeng: 2016, *Astrophys Space Sci.,* **361**, 306